J|A|C|S ARTICLES

Published on Web 04/28/2010

Inhibition of the Fe_4S_4-Cluster-Containing Protein IspH (LytB): Electron Paramagnetic Resonance, Metallacycles, and Mechanisms

Ke Wang,[†] Weixue Wang,[‡] Joo-Hwan No,[‡] Yonghui Zhang,[†] Yong Zhang,[§] and Eric Oldfield*[,†,‡]

Department of Chemistry, 600 South Mathews Avenue, and Center for Biophysics and Computational Biology, 607 South Mathews Avenue, University of Illinois at Urbana−Champaign, Urbana, Illinois 61801, and Department of Chemistry and Biochemistry, University of Southern Mississippi, 118 College Drive No. 5043, Hattiesburg, Mississippi 39406

Received November 30, 2009; E-mail: eo@chad.scs.uiuc.edu

Abstract: We report the inhibition of the *Aquifex aeolicus* IspH enzyme (LytB, (*E*)-4-hydroxy-3-methyl-but-2-enyl diphosphate reductase, EC 1.17.1.2) by a series of diphosphates and bisphosphonates. The most active species was an alkynyl diphosphate having $IC_{50} = 0.45\ \mu M$ ($K_i \approx 60$ nM), which generated a very large change in the 9 GHz EPR spectrum of the reduced protein. On the basis of previous work on organometallic complexes, together with computational docking and quantum chemical calculations, we propose a model for alkyne inhibition involving π (or π/σ) "metallacycle" complex formation with the unique fourth Fe in the Fe_4S_4 cluster. Aromatic species had less activity, and for these we propose an inhibition model based on an electrostatic interaction with the active site E126. Overall, the results are of broad general interest since they not only represent the first potent IspH inhibitors but also suggest a conceptually new approach to inhibiting other Fe_4S_4-cluster-containing proteins that are of interest as drug and herbicide targets.

Introduction

The Rohmer, methyl-D-erythritol phosphate, or non-mevalonate pathway is responsible for isoprenoid biosynthesis in most pathogenic bacteria, as well as in malaria parasites.[1,2] Since isoprenoids are essential for survival in these organisms and since the non-mevalonate pathway is absent in humans, enzymes that comprise the pathway are important anti-infective drug targets,[3,4] and in previous work[5,6] it was shown that fosmidomycin (which inhibits the second enzyme in the pathway) gave very promising results for treating malaria. The structures and mechanisms of action of six of the eight enzymes present in the pathway have been known for some time, but deducing the structures (and mechanisms of action) of the last two enzymes has been more challenging. The penultimate enzyme is *E*-4-hydroxy-3-methyl-but-2-enyl diphosphate (HMBPP) synthase (IspG, GcpE, EC 1.17.7.1), which catalyzes the $2H^+/2e^-$ reduction of 2-*C*-methylerythritol-2,4-*cyclo*-diphosphate (MEcPP, **1**) to HMBPP (**2**), while the terminal enzyme, HMBPP reductase (IspH, LytB, EC 1.17.1.2), catalyzes the $2H^+/2e^-$ reduction of HMBPP to isopentenyl diphosphate (IPP, **3**) and dimethylallyl diphosphate (DMAPP, **4**) in a ~5:1 ratio.

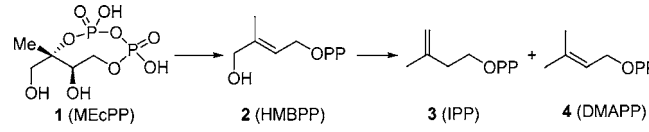

1 (MEcPP) **2** (HMBPP) **3** (IPP) **4** (DMAPP)

The structure of IspG has not yet been reported, but there have been two structures published for IspH, one from *Aquifex aeolicus*[7] and the other from *Escherichia coli*.[8] Both structures contain Fe_3S_4 clusters. However, on the basis of the results of Mössbauer[9,10] and electron paramagnetic resonance (EPR) spectroscopy[11] and from microchemical analyses,[9,11] we and others have concluded that Fe_4S_4 clusters are responsible for catalysis. The Fe_4S_4 cluster, while catalytically active, is thus relatively labile, as also found, for example, in aconitase and

[†] Department of Chemistry, University of Illinois at Urbana−Champaign.
[‡] Center for Biophysics and Computational Biology, University of Illinois at Urbana−Champaign.
[§] University of Southern Mississippi.

(1) Rohmer, M. *Lipids* **2008**, *43*, 1095.
(2) Wiesner, J.; Jomaa, H. *Curr. Drug Targets* **2007**, *8*, 3.
(3) Williams, S. L.; McCammon, J. A. *Chem. Biol. Drug. Des.* **2009**, *73*, 26.
(4) de Ruyck, J.; Wouters, J. *Curr. Protein Pept. Sci.* **2008**, *9*, 117.
(5) Jomaa, H.; Wiesner, J.; Sanderbrand, S.; Altincicek, B.; Weidemeyer, C.; Hintz, M.; Turbachova, I.; Eberl, M.; Zeidler, J.; Lichtenthaler, H. K.; Soldati, D.; Beck, E. *Science* **1999**, *285*, 1573.
(6) Borrmann, S.; Lundgren, I.; Oyakhirome, S.; Impouma, B.; Matsiegui, P. B.; Adegnika, A. A.; Issifou, S.; Kun, J. F. J.; Hutchinson, D.; Wiesner, J.; Jomaa, H.; Kremsner, P. G. *Antimicrob. Agents Chemother.* **2006**, *50*, 2713.
(7) Rekittke, I.; Wiesner, J.; Rohrich, R.; Demmer, U.; Warkentin, E.; Xu, W.; Troschke, K.; Hintz, M.; No, J. H.; Duin, E. C.; Oldfield, E.; Jomaa, H.; Ermler, U. *J. Am. Chem. Soc.* **2008**, *130*, 17206.
(8) Grawert, T.; Rohdich, F.; Span, I.; Bacher, A.; Eisenreich, W.; Eppinger, J.; Groll, M. *Angew. Chem., Int. Ed.* **2009**, *48*, 5756.
(9) Xiao, Y.; Chu, L.; Sanakis, Y.; Liu, P. *J. Am. Chem. Soc.* **2009**, *131*, 9931.
(10) Seemann, M.; Janthawornpong, K.; Schweizer, J.; Bottger, L. H.; Janoschka, A.; Ahrens-Botzong, A.; Tambou, E. N.; Rotthaus, O.; Trautwein, A. X.; Rohmer, M.; Schunemann, V. *J. Am. Chem. Soc.* **2009**, *131*, 13184.
(11) Wolff, M.; Seemann, M.; Bui, B. T. S.; Frapart, Y.; Tritsch, D.; Garcia Estrabot, A.; Rodriguez-Concepcion, M.; Boronat, A.; Marquet, A.; Rohmer, M. *FEBS Lett.* **2003**, *541*, 115.

in pyruvate−formate lyase activating enzyme.[12] To date, there has been only one report of IspH inhibitors,[13] with IC_{50} values of ~1−2 mM having been obtained. Here, we report progress aimed at obtaining more potent inhibitors.

On the basis of the crystallographic, mutagenesis, catalytic activity, and spectroscopic results described previously,[7−11] we reasoned that there might be two distinct approaches to developing IspH inhibitors. In the first, it might be possible to develop "conventional" inhibitors which bind to amino acids involved in catalysis. In previous work[7] we proposed that a key residue involved in delivering H^+ to HMBPP was the totally conserved E126, and the essential nature of this residue in catalysis has now been confirmed by site-directed mutagenesis.[8] We reasoned that basic or cationic inhibitors might interact with this key residue, inhibiting the enzyme. The second hypothesis to test is that "unconventional" inhibitors, compounds that bind to the Fe/S cluster, might be developed. If the cluster is Fe_3S_4, this would be unprecedented and would thus, of course, not suggest what inhibitor structures to make. On the other hand, if the active species is Fe_4S_4 (as deduced from the IspH Mössbauer,[9,10] EPR,[11] and catalytic activity[9,11] results), there is in fact precedent for the formation of organometallic species (i.e., containing Fe−C bonds) between Fe_4S_4 clusters and alkynes, which would be expected to act as IspH inhibitors. For example, in the early literature, McMillan et al.[14] investigated the reduction of acetylene (C_2H_2) to ethylene (C_2H_4) by reduced Fe_4S_4 synthetic clusters, in particular $[Fe_4S_4(SPh)_4]^{3-}$ (**5**). These workers proposed that an acetato complex reacted initially with C_2H_2 to form an organometallic species, **6**, most likely containing a side-on (π/σ) acetylene unit, which was then *cis*-reduced to ethylene. Basically the same reduction, of diphenylacetylene (**7**) to *cis*-stilbene (**8**), was reported by Itoh.[15] In these systems, the alkyne complex was not observed directly, but under controlled potential (electrochemical reduction) conditions, Tanaka et al.[16] found evidence for a π complex of acetylene bound to $[Fe_4S_4(SPh)_4]^{3-}$ and $[Mo_2Fe_6S_8(SPh)_9]^{3-}$ clusters, as evidenced by quite large shifts in the C≡C vibrational Raman spectra. These workers also demonstrated that acetylene bound most strongly to reduced ($[Fe_4S_4]^+$) clusters, which resulted in release of one SPh^-. These results suggested to us that acetylenes might likewise bind to reduced IspH, forming organometallic (Fe−C) bonds. Interestingly, with low-valent (Fe^I) complexes, alkynes have also been found to bind far more strongly than do alkenes,[17] leading again to the possibility that alkynes could bind to Fe and be good IspH inhibitors, displacing the olefinic substrate, HMBPP.

$$\underset{\mathbf{5}}{[Fe_4S_4(SPh)_4]^{3-}} \xrightarrow{OAc^-} [Fe_4S_4(SPh)_3(OAc)]^{3-} + SPh^- \xrightarrow{C_2H_2} \underset{\mathbf{6}}{[Fe_4S_4(SPh)_3(C_2H_2)]^{2-}} + OAc^-$$

This formation of a π (or π/σ) "metallacycle" complex would be very similar to that deduced for the binding of the HMBPP parent molecule, allyl alcohol (which lacks the Me and CH_2OPP substituents), to the FeMo cofactor in nitrogenase,[18] illustrated schematically above (**9**) as the Fe_3MoS_3X cubane-like fragment. It also seemed possible that aromatic residues might interact with the Fe_4S_4 cluster, just as the cyclopentadienide ion does in model Fe_4S_4 clusters,[19] such as **10** (as an η^6 as opposed to an η^5 species). Although the structures of complexes such as **6** have not been confirmed crystallographically, the structure proposed by McMillan et al.[14] (**6**) is likely to involve the same type of bonding as found in many other organometallic complexes,[20] being described[18] as a resonance hybrid of a pure π complex and a σ complex, the latter corresponding to a metallacycle.

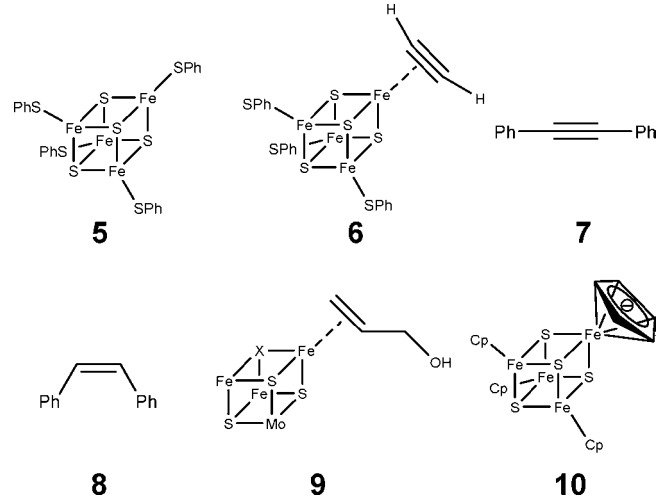

5 **6** **7** **8** **9** **10**

Results and Discussion

In an effort to learn more about just what types of compound might bind to the Fe_4S_4 cluster in IspH, we first screened a series of small molecules using EPR spectroscopy. The 9 GHz EPR spectrum of *A. aeolicus* IspH in the $g \approx 2$ region exhibits a broad signal (Figure 1a), very similar to that of the *E. coli* protein (Figure 1b), and is characteristic of an $S = 1/2$ $[Fe_4S_4]^+$ species.[11] The unliganded *A. aeolicus* IspH also has two small signals at $g \approx 5$ (Supporting Information Figure S1a), which likely indicate the presence of higher spin species. For the purpose of comparison, the *g*-values for the systems studied here are presented in Supporting Information Table S1, together with *g*-values for related systems such as aconitase and IspG (GcpE).

We first tested a series of small molecules and ions, CO, N_3^-, MeCN, and CN^-, for cluster-binding in *A. aeolicus* IspH, but only CN^- was found to have any effect on the EPR spectrum (Figure 1c and Supporting Information Figure S1b). The *g*-values observed were 2.08/2.05 and 1.94 (Figure 1c), close to those observed previously with CN^- binding to the *Pyrococcus furiosus* 4Fe ferredoxin ($g_1 = 2.09$, $g_2 = 1.95$, and $g_3 = 1.92$), another 4Fe-4S cluster with three Cys ligands and a unique fourth Fe position,[21] due, we propose, to end-

(12) Mulliez, E.; Ollagnier-de Choudens, S.; Meier, C.; Cremonini, M.; Luchinat, C.; Trautwein, A. X.; Fontecave, M. *J. Biol. Inorg. Chem.* **1999**, *4*, 614.
(13) Van Hoof, S.; Lacey, C. J.; Rohrich, R. C.; Wiesner, J.; Jomaa, H.; Van Calenbergh, S. *J. Org. Chem.* **2008**, *73*, 1365.
(14) McMillan, R. S.; Renaud, J.; Reynolds, J. G.; Holm, R. H. *J. Inorg. Biochem.* **1979**, *11*, 213.
(15) Itoh, T.; Nagano, T.; Hirobe, M. *Tetrahedron Lett.* **1980**, *21*, 1343.
(16) Tanaka, K.; Nakamoto, M.; Tsunomori, M.; Tanaka, T. *Chem. Lett.* **1987**, 613.
(17) Yu, Y.; Smith, J. M.; Flaschenriem, C. J.; Holland, P. L. *Inorg. Chem.* **2006**, *45*, 5742.
(18) Pelmenschikov, V.; Case, D. A.; Noodleman, L. *Inorg. Chem.* **2008**, *47*, 6162.
(19) Schunn, R. A.; Fritchie, C. J., Jr.; Prewitt, C. T. *Inorg. Chem.* **1966**, *5*, 892.
(20) Crabtree, R. H. *The Organometallic Chemistry of the Transition Metals*, 4th ed.; John Wiley & Sons, Inc.: Hoboken, NJ, 2005; Chapters 3 and 5.
(21) Telser, J.; Smith, E. T.; Adams, M. W. W.; Conover, R. C.; Johnson, M. K.; Hoffman, B. M. *J. Am. Chem. Soc.* **1995**, *117*, 5133.

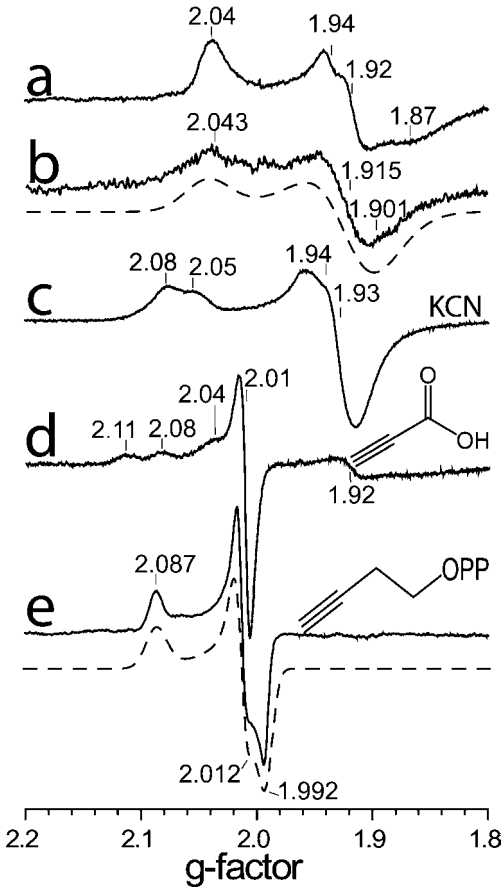

Figure 1. 9 GHz EPR spectra of IspH at 15 K, reduced with $Na_2S_2O_4$. (a) *A. aeolicus* IspH, no added ligands, microwave power = 1 mW. (b) *E. coli* IspH, no added ligands, microwave power = 1 mW. (c) *A. aeolicus* IspH + KCN, 10 equiv, microwave power = 1 mW. (d) *A. aeolicus* IspH + propiolic acid, 10 equiv, microwave power = 0.2 mW. (e) *A. aeolicus* IspH + but-3-ynyl diphosphate (**12**), 20 equiv, microwave power = 0.05 mW. Spectral simulations are shown by the dashed lines. (*g*-values are compiled in Supporting Information Table S1, together with g-values for Fe_3S_4 proteins.)

on binding to the fourth Fe in IspH. There was also an increase in signal intensity in the $g \approx 2$ region (from ~20% to ~60% spin/protein) due to conversion of the higher spin state species to $S = 1/2$.

We then tested a series of other small molecules that might be anticipated to bind in a sideways-on mode (as proposed for acetylene in the model systems): propargyl alcohol, propargylamine, and propiolic acid. All species resulted in large spectral changes, and by way of example the IspH + propiolic acid ($HC{\equiv}CCO_2H$) spectrum is shown in Figure 1d. These results indicated to us that, as with the Fe_4S_4-containing small molecules, acetylenes bind to IspH, forming π or π/σ complexes. With CN^- as well as propiolic acid binding, there also appear to be two bound ligand conformations or binding modes (e.g., hydrogen-bonded or not), as evidenced by the splitting of the g_1 signals.

However, propiolic acid had poor activity in IspH inhibition, and we reasoned that acetylenic diphosphates (or the isoelectronic cyano diphosphates) might interact more strongly with IspH, since there would be an increase in binding affinity due to their diphosphate moieties docking into the (inorganic) PPi site seen crystallographically.[8] We thus synthesized four acetylenic diphosphates (**11**−**14**, Figure 2) and two cyanoalkyl diphosphates (**15** and **16**) and tested them for their activity in IspH inhibition. IC_{50} results are shown in Figure 2. The most active compound was **12**, with $IC_{50} = 0.45\ \mu M$ ($K_i \approx 60$ nM, Figure 3a). As shown in Figure 3b, this compound can bind with its diphosphate group in the inorganic "PPi" site seen crystallographically,[8] with the alkyne fragment interacting with the unique fourth Fe (identified from EPR, Mössbauer, and catalytic activity results, and added computationally here as described previously[7]), with Fe−C bond lengths of ~2.4 Å, suggesting π complex formation. There was a large change in the EPR spectrum of IspH in the presence of **12** (Figure 1e and Supporting Information Figure S1c), indicating a major change in the cluster's electronic structure, consistent with these docking results. Moreover, there was evidence for only a single bound species. The shorter chain analogue **11** was less active than **12**, as was the longer chain analogue **13**, and conversion of the bridging O to CH_2 (**17**) reduced the activity of **11** even more (Figure 2), due presumably to a disruption in H-bonding to the SXN motif. Likewise, the addition of a terminal CH_2OH (**14**) reduced activity, consistent with the known stronger binding of terminal versus substituted alkynes to low-valent Fe complexes.[17] The changes in *g*-values on addition of the acetylenes were generally similar, as expected, and as with CN^- there was an ~3-fold increase in signal intensity in the $g \approx 2$ region (due to a high-to-low spin state conversion).We also tested the effects of the isoelectronic analogues (**15** and **16**) of the acetylenes (−C≡C−H → −C≡N), cyanides, on IspH inhibition, but both compounds were far less active than their acetylenic counterparts.

These results clearly indicate that alkyne diphosphates can be good IspH inhibitors, with the most active species being >1000 times more potent than previously reported IspH inhibitors.[13] Since PPi itself and other diphosphates are only weak (~1 mM) IspH inhibitors,[8] we conclude that ligand binding is driven by π (or π/σ) or η^2-alkynyl complex formation with the Fe_4S_4 cluster, the same type of complex formation as suggested by Raman spectroscopy,[16] for acetylene binding to an $[Fe_4S_4(SPh)_4]^{3-}$ cluster. Moreover, the results of density functional theory (DFT) calculations show that there is indeed Fe−C metal−ligand bonding present in an $[Fe_4S_4(SMe)_3(HC{\equiv}CCH_2OH)]^{2-}$ model system. We show in Figure 3c,d some typical molecular orbital results. The αHOMO−1 shows the interaction of an Fe d orbital with the C≡C π orbital, in the plane of the Fe···C≡C fragment. The βHOMO−1 illustrates the interaction between an Fe d orbital and another type of C≡C π orbital, this time perpendicular to the plane of Fe···C≡C. If IspH, under these reducing conditions, contained an Fe_3S_4 cluster, there would be no obvious way in which acetylenes would bind tightly to the cluster (or the protein), while η^2-alkynyl (i.e., π or π/σ) complex formation is predicted on the basis of previous work and is supported by the DFT results.

We next investigated a series of cationic (or basic) diphosphates and (cationic) bisphosphonates, which are isosteres of the diphosphate group. In previous work[22] we found that aromatic, cationic bisphosphonates (such as **18**)

(22) Sanders, J. M.; et al. *J. Med. Chem.* **2005**, *48*, 2957.

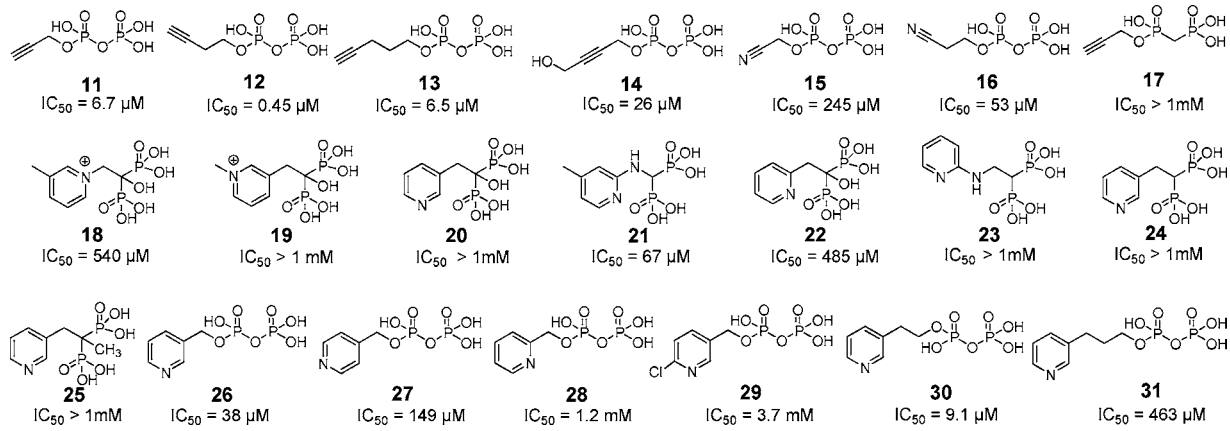

Figure 2. Structures of the 21 compounds investigated as *A. aeolicus* IspH inhibitors, together with (below the structures) their IC_{50} values.

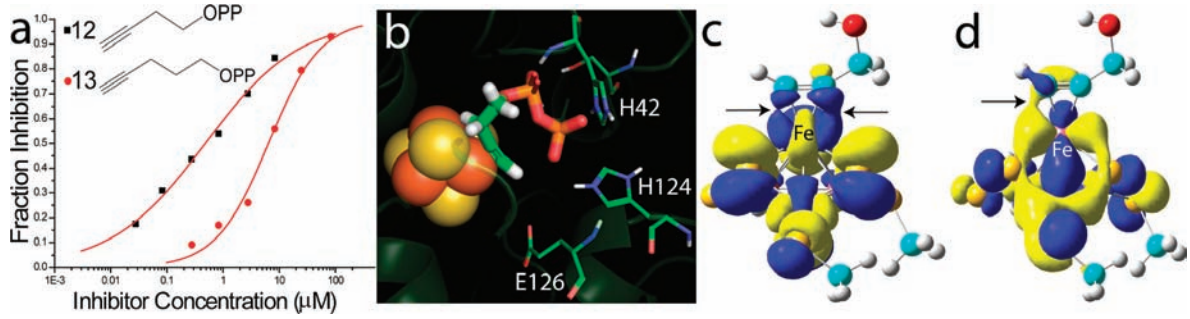

Figure 3. IspH inhibition by alkyne diphosphates. (a) Dose−response curves for IspH inhibition by **12** (IC_{50} = 450 nM) and **13** (IC_{50} = 6.5 μM). (b) Proposed docking model for **12** bound to the IspH active site: the diphosphate binds to the PPi site, while the alkyne group forms a π (or π/σ) "metallacycle" complex with the unique fourth Fe in the Fe_4S_4 cluster, similar to that proposed for acetylene binding to model Fe_4S_4 clusters and allyl alcohol binding to a nitrogenase FeMo cofactor. (c) αHOMO−1 for propargyl alcohol bound to a model Fe_4S_4 cluster, illustrating metal−ligand interaction. (d) Same as in part c but βHOMO−1. The contour values are ±0.02 au.

were potent ($K_i \approx 20$ nM) inhibitors of the enzyme farnesyl diphosphate synthase since, as shown below,

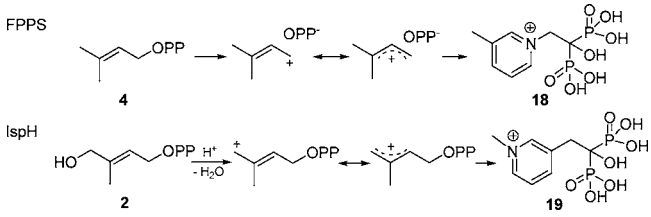

their charge distribution mimics that expected for the allylic cation/diphosphate anion ion-pair.[23] In the case of IspH, similar allylic cations (shown above) have been proposed[24] to be involved in catalysis, so we tested both **18** and **19** for their activities in IspH inhibition. Neither had potent activity (**18**, IC_{50} = 540 μM; **19**, IC_{50} > 1 mM, Figure 2). We then tested six additional bisphosphonates (**20**−**25**, Figure 2) with 1-H, 1-Me, or 1-OH backbone groups and pyridine, pyridinium, or amino-pyridine side chains. The most active compound (IC_{50} = 67 μM) was **21**, an amino-pyridine, expected to contain an amidinium-like (protonated) side chain. Overall, however, the activity of these bisphosphonates was only modest, and on the basis of Glide[25] docking results using the "closed" IspH structure (PDB file 3F7T), it appeared that this might be due to the "branched" nature of the bisphosphonate backbone. We thus next synthesized a series of pyridinium diphosphates, **26**−**29**, which on the basis of computational docking results using Glide appeared to better fit the IspH active site. The most active compound in the series (Figures 2 and 4a) was **26**, a *m*-pyridinium diphosphate having IC_{50} = 38 μM, slightly more potent than the best bisphosphonate, **21**. We find that, when docked into the IspH active site (Figure 4b,c), the diphosphate backbone binds to the "PPi" site seen crystallographically, and the pyridinium H^N is only ~1.9 Å from the E126 O (modeled as CO_2^-), indicating the possibility of an H-bond or electrostatic interaction with this active-site residue. The *p*-pyridinium analogue **27** was less active (IC_{50} = 149 μM), and the *o*-pyridinium analogue **28** was far less active (IC_{50} = 1.2 mM), correlating with the increased NH−O (CO_2^-) distances of 3.47 and 4.28 Å (Figure 4c). Interestingly, all three aromatic rings also locate close to the fourth Fe, but the major decrease in activity seen as the ring nitrogens move away from the E126 carboxyl indicates the dominance of a Coulombic interaction, consistent with the lack of activity of the chloropyridine analogue, **29**, which is expected to be far less basic than is **26**. These activity and docking results are consistent, then, with the pyridinium diphosphates binding to IspH with their PPi groups binding to the inorganic PPi site, while their aromatic rings interact with E126, as illustrated in Figure 4b,c. There was no major change in the EPR spectrum of **26** bound to the protein (Supporting Information Figure S1d), consistent with the lack of any π complex interaction. We then sought to improve activity by varying the length of the CH_2 spacer in the side chain: addition of one CH_2 group (**30**) resulted in IC_{50} = 9.1 μM ($K_i \approx 1.2$ μM), but addition of two CH_2 groups reduced

(23) Martin, M. B.; Arnold, W.; Heath, H. T., III; Urbina, J. A.; Oldfield, E. *Biochem. Biophys. Res. Commun.* **1999**, *263*, 754.
(24) Altincicek, B.; Duin, E. C.; Reichenberg, A.; Hedderich, R.; Kollas, A. K.; Hintz, M.; Wagner, S.; Wiesner, J.; Beck, E.; Jomaa, H. *FEBS Lett.* **2002**, *532*, 437.
(25) *Glide 4.5*; Schrodinger, LLC: New York, 2007.

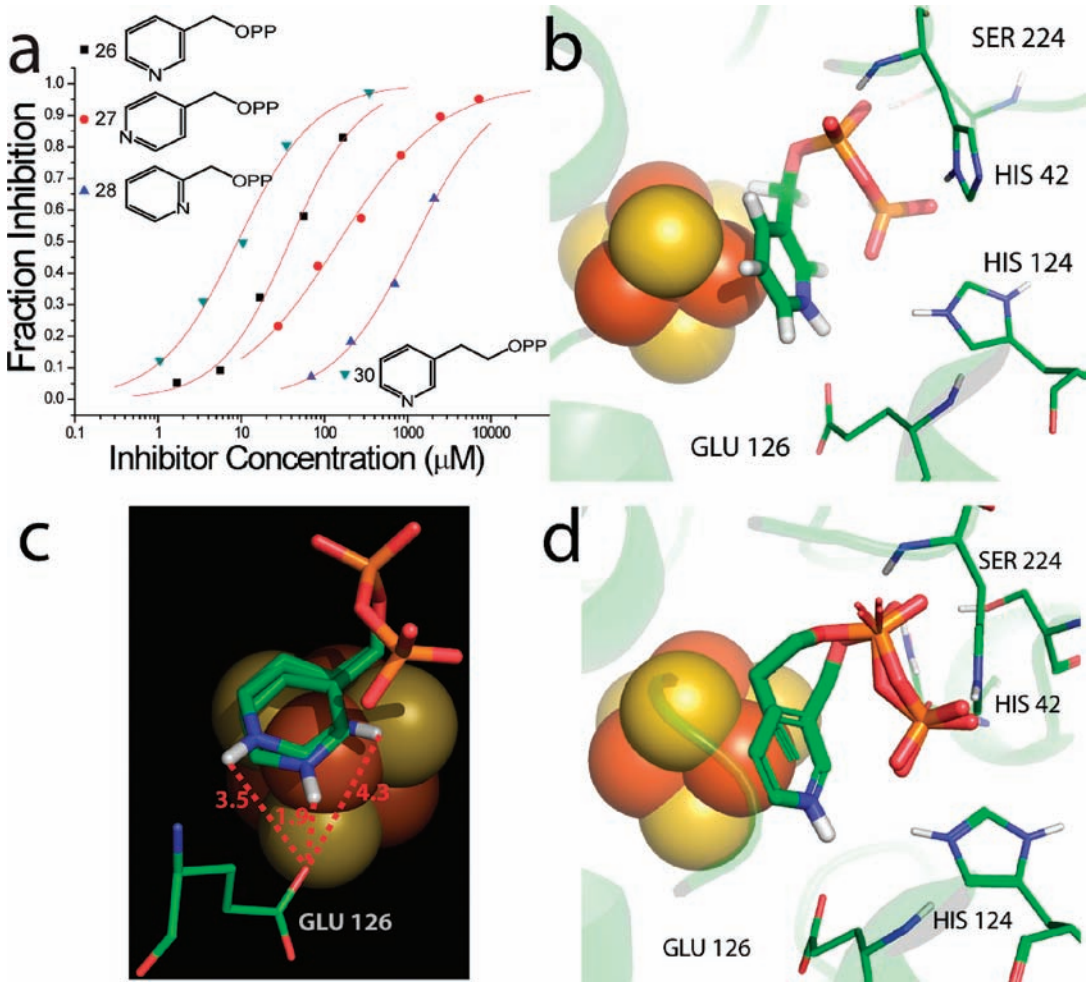

Figure 4. IspH inhibition by pyridinium diphosphates. (a) Dose−response curves for IspH inhibition by **26**, **27**, **28**, and **30**. The IC_{50} for the most potent inhibitor (**30**) is 9.1 μM; $K_i \approx 1.2$ μM. (b) Glide docking pose for **26** bound to the IspH active site: the diphosphate binds to the PPi site, while the pyridinium side chain interacts with E126. (c) View of the *o*-, *m*-, and *p*-pyridinium diphosphates (**26**−**28**) docked to IspH: the most potent inhibitor has the shortest $H^N\cdots$E126 CO_2^- distance; the worst inhibitor has the longest distance. (d) Superimposed docking poses for **12** and **26**, showing that they both bind in the same region (preventing HMBPP binding).

activity (**31**, IC_{50} = 463 μM; Figure 2), with the pyridinium nitrogen in **30** again docking close to E126, while in **31** it did not. Taken together, these results argue against formation of a carbocation mechanism since, for this, we would anticipate good activity for **28** (with maximum charge density separated by two carbons from the PPi backbone), while experimentally, maximum activity is found with **30** (with its NH^+ located four carbons from the PPi backbone). That is, none of the cationic (**18** and **19**) or pyridine/pyridinium analogues of the putative carbocation transition states (or reactive intermediates) act as inhibitors, while the longer-chain species that can bind to both the PPi site and E126 are the most potent inhibitors among the whole series of compounds (**18**−**31**) investigated. Notably, with both the alkyne and the cationic inhibitors, the side chains are located (Figure 4d) close to the Fe_4S_4 cluster, blocking, we propose, HMBPP access.

These results lead to the proposals for IspH inhibition shown in Figure 5. We propose that both alkyne and alkene diphosphates (i.e., HMBPP) bind to the Fe_4S_4 cluster at the unique fourth Fe, forming π (or π/σ) "metallacycles", as shown in Figure 5a,b, the same type of binding reported previously for the HMBPP parent molecule (allyl alcohol) bound to the FeMo cofactor in nitrogenase.[18] As shown in Figure 5b, the presence of such a metallacycle also immediately leads to a proposal for the IspH catalytic mechanism in which, in a first H^+/e^- step, the HMBPP 4-OH is protonated and an η^1-allyl intermediate and water form. This intermediate is then cleaved in a second H^+/e^- step, forming the DMAPP product (Figure 5b). IPP forms in the same way, after an η^1-allyl (or η^3-allyl) isomerization. This model is described in more detail elsewhere[26] and is supported by electron nuclear double-resonance (ENDOR) spectroscopy using [u-^{13}C]- and [^{2}H]-labeled HMBPP, which strongly suggests metal−ligand interaction. We thus propose that the alkyne as well as the cationic inhibitors block or displace HMBPP from binding to the Fe_4S_4 cluster: the alkynes form π (or π/σ) "η^2-alkynyl" metallacycles, while the cationic inhibitors interact with the active-site E126 carboxylate, again effectively blocking HMBPP binding.

Validation of the Mechanism of IspH Inhibition and Catalysis. Finally, during the review of this article, Grawert et al.[27] reported the results of new crystallographic structures of HMBPP, PPi, IPP, and DMAPP bound to IspH[27] which help us validate the inhibition models proposed here. These workers

(26) Wang, W.; Wang, K.; Liu, Y.-L.; No, J. H.; Nilges, M. J.; Oldfield, E. *Proc. Natl. Acad. Sci. U.S.A.* **2010**, *107*, 4522.
(27) Grawert, T.; Span, I.; Eisenreich, W.; Rohdich, F.; Eppinger, J.; Bacher, A.; Groll, M. *Proc. Natl. Acad. Sci. U.S.A.* **2010**, *107*, 1077.

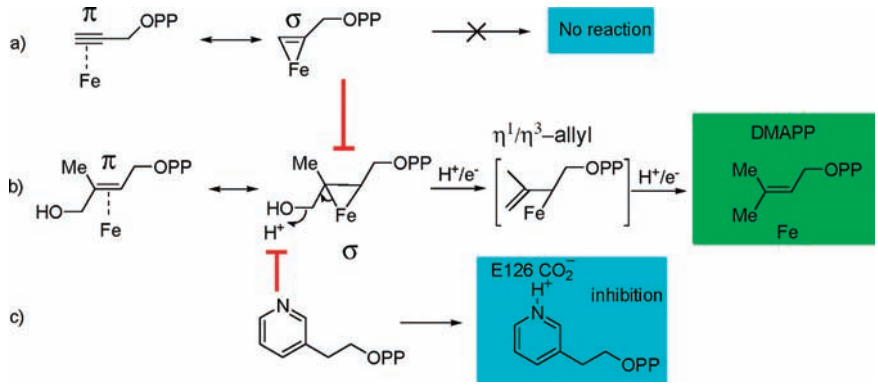

Figure 5. Mechanistic proposals for IspH catalysis and inhibition. (a) π (or π/σ) metallacycle complex formation by alkyne inhibitors. (b) IspH catalysis in which an η^2-alkenyl metallacycle is reduced and protonated and then dehydrates to form an allyl complex, which is then cleaved to form the DMAPP and IPP products. (c) IspH inhibition by pyridinium diphosphates which block HMBPP binding to the fourth Fe.

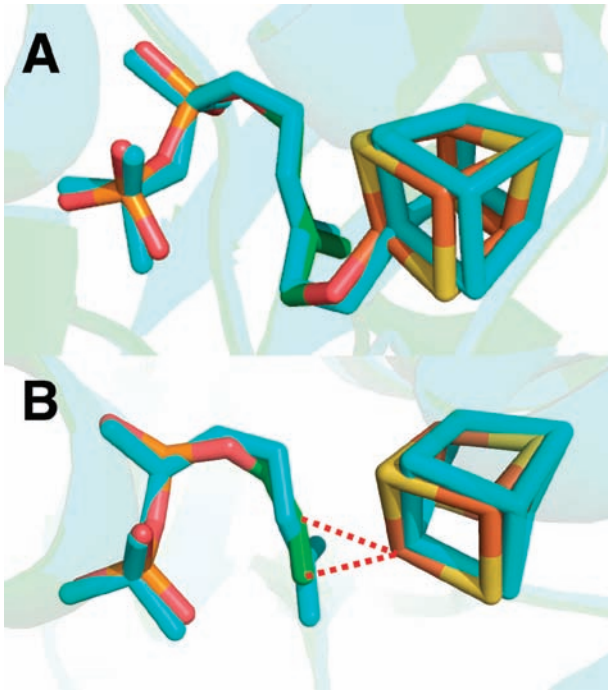

Figure 6. Comparisons between X-ray structures and docking/EPR/ENDOR-deduced structures for (A) HMBPP initial docking (PDB code 3KE8, and ref 25 Figure 1G) and (B) propargyl diphosphate (docking) superimposed on deoxy complex (PDB ID code 3KE9, and ref 25 Figure 5).

now report that HMBPP binds as an alkoxide to the unique fourth iron (to the oxidized $[Fe_4S_4]^{2+}$ cluster), the same binding mechanism we proposed earlier.[7] On irradiation in the X-ray beam, HMBPP is reduced, forming a deoxy species (bound to the Fe_4S_4 cluster), basically as we proposed on the basis of EPR/ENDOR and docking results.[26] These X-ray results are of interest since they enable us to make a direct comparison between the X-ray and EPR/ENDOR/docking-based methods,[26,27] helping us validate the use of inhibitor docking. We show in Figure 6A an alignment of the X-ray structure of HMBPP bound to IspH with that we proposed (Figure 1G in ref 26) for the initial HMBPP binding pose, in which the O-4 can interact with the unique fourth Fe. There is a 0.32 Å rmsd between the heavy atoms (C, O, P) in the HMBPP ligand between the X-ray and our docking/EPR-based structures, ~0.43 Å if we include the Fe and S atoms in the cluster (Figure 6A). On reduction, the 4-OH is removed from the ligand and the σ/π metallacycle is reduced, resulting in loss of water and formation of η^1/η^3-allyl complexes, and thence IPP and DMAPP.[26,27]

The new crystallographic results are thus in good accord with those we proposed from our EPR, ENDOR, and computational work, which gives confidence in the proposed ligand geometries we describe here for the bound inhibitors. As can be seen in Figure 6B, the alkyne group in propargyl diphosphate (**11**) bound to IspH[26] is located in essentially the same position as the deoxy product species seen crystallographocally, where it can interact with the unique fourth iron, forming a π or π/σ complex. The alkynes are much stronger inhibitors of IspH than are the alkenes (IPP, DMAPP),[8] and indeed the ENDOR spectrum of **11** bound to IspH exhibits an ~6 MHz ^{13}C hyperfine interaction,[26] 2−3 times larger than the ^{13}C hyperfine interactions found for either allyl alcohol bound to nitrogenase[28] or HMBPP bound to IspH.[26]

Conclusions

Taken together, these results are of interest for several reasons. First, we find that cationic diphosphates are IspH inhibitors. However, rather than mimicking transition states/reactive intermediates, we propose that they interact with the active-site E126, preventing HMBPP binding to the Fe_4S_4 cluster. Second, we find that alkyne diphosphates are quite potent ($IC_{50} \approx 0.45$ μM; $K_i \approx 60$ nM) IspH inhibitors. This activity was predicted on the basis of previous Raman and catalytic activity results with model systems, which have been interpreted as indicating π (or π/σ) "metallacycle" formation between Fe_4S_4 clusters and acetylene. That alkynes are, in fact, IspH inhibitors also supports the idea that catalytically active IspH contains active-site Fe_4S_4 and not Fe_3S_4 clusters, since there is no obvious way in which an alkyne group would bind to the three exposed S^{2-} in such clusters. On the other hand, there is good literature precedent for alkynes binding to Fe_4S_4 clusters, supporting formation in IspH of π (or π/σ) complex formation. Third, the results of quantum chemical calculations indicate Fe−C metal ligand bonding with the acetylene group (in an $[Fe_4S_4(SMe)_3(HC{\equiv}CCH_2OH)]^{2-}$ model). Fourth, the formation of acetylene metallacycles is consistent with the observation that the HMBPP parent molecule, allyl alcohol, forms a metallacycle with the nitrogenase FeMo cofactor, which contains a related Fe/S (Mo, "X") cluster and where the ligand forms Fe−C bonds with a single Fe. The observation that the IC_{50} for the most potent IspH

(28) Lee, H. I.; Igarashi, R. Y.; Laryukhin, M.; Doan, P. E.; Dos Santos, P. C.; Dean, D. R.; Seefeldt, L. C.; Hoffman, B. M. *J. Am. Chem. Soc.* **2004**, *126*, 9563.

alkyne inhibitor ($IC_{50} = 0.45\ \mu M$; $K_i \approx 60$ nM) is much smaller than the K_M for HMBPP binding ($K_M = 5\ \mu M$) is also expected on the basis of organometallic precedent in which alkynes bind much more strongly (to low-valent Fe complexes) than do alkenes.[17] Fifth, we find that CN^- binds to IspH with the resulting spectrum quite strongly resembling that found with *P. furiosus* Fd, another protein with a unique fourth Fe. And finally, the recent revision of the earlier three Fe IspH structural/mechanistic models is in accord with our earlier mechanistic proposal of initial binding of the HMBPP 4-OH (as an alkoxide) to an $[Fe_4S_4]^{2+}$ cluster which, on reduction, forms an allyl complex that is then cleaved to form the IPP and DMAPP products.[26] This gives confidence in the models we propose here for alkyne inhibition. These results also open up the intriguing possibilities that metallacycle complexes may act as reactive intermediates (or transition states) in both IspG and IspH catalysis and that alkynes can be expected to be good inhibitors of other Fe_4S_4-cluster-containing enzymes which contain "unique" fourth Fe atoms.

Materials and Methods

***A. aeolicus* IspH Protein Purification.** BL-21(DE3) cells expressing IspH from *A. aeolicus* were grown in LB media supplemented with 150 mg/mL ampicillin at 37 °C until the OD_{600} reached 0.6. Cells were then induced with 200 μg/L anhydrotetracycline and then grown at 20 °C for 15 h. Cells were harvested by centrifugation (9000 rpm, 8 min, 4 °C) and kept at −80 °C until use. Cell pellets were resuspended and lysed in B-PER (Thermo Scientific, Rockford, IL) protein extraction reagent for 1 h at 4 °C and then centrifuged at 200 000 rpm at 4 °C for 15 min. The supernatant was applied to a Ni-NTA column equilibrated with 5 mM imidazole in pH 8.0 buffer containing 50 mM Tris·HCl and 150 mM NaCl. After washing with 20 mM imidazole, protein was eluted with 100 mM imidazole. Fractions were collected and dialyzed in pH 8.0 buffer containing 50 mM Tris·HCl, 150 mM NaCl, 5% glycerol, and 1 mM DTT, four times. The purified protein was flash-frozen in liquid nitrogen and stored at −80 °C until use.

***E. coli* IspH Protein Purification.** BL21 DE3 (Invitrogen) cells harboring an *E. coli* IspH construct were grown in LB media at 37 °C until the OD_{600} reached 0.6. Induction was performed with 200 ng/mL anhydrotetracycline at 20 °C for 15 h. Cells were harvested by centrifugation at 9000 rpm for 8 min and stored at −80 °C. Cell pellets were resuspended and lysed in B-PER protein extraction reagent for about 1 h at 4 °C, and then the lysate was centrifuged at 250 000 rpm for 30 min. The supernatant was collected and loaded onto an IBA Strep-tag column equilibrated with buffer W (100 mM Tris·HCl, 150 mM NaCl, pH 8.0). After washing with buffer W, protein was eluted using buffer E (buffer W containing 2.5 mM desthiobiotin). Fractions were collected and dialyzed in pH 8.0 buffer containing 50 mM Tris·HCl, 150 mM NaCl, 5% glycerol, and 1 mM DTT, twice. The purified protein was flash-frozen in liquid nitrogen and stored at −80 °C until use.

Protein Reconstitution. Both *A. aeolicus* and *E. coli* IspH proteins as isolated had a very small peak at 410 nm ($A_{280}/A_{410} < 0.02$), so they were reconstituted for further studies. Before reconstitution, protein was transferred into a Coy vinyl anaerobic chamber after being degassed on a Schlenk line. The following steps were performed inside the anaerobic chamber with an oxygen level <2 ppm. In a typical reconstitution experiment, 10 mM DTT and ∼0.5 mg of elemental sulfur were added to 3 mL of 0.6 mM protein solution in a pH 8.0 buffer containing 50 mM Tris·HCl, 150 mM NaCl, and 5% glycerol. After 1.5 h under stirring, $FeCl_3$ was slowly added from a 30 mM stock solution to 6 equiv. After 3 h, an aliquot of the solution was centrifuged and a UV−vis spectrum recorded. If the $A_{410\ nm}/A_{280\ nm}$ ratio was ≥0.38, the protein was then desalted by passing through a PD10 column. If the ratio was <0.38, more DTT, elemental sulfur, and $FeCl_3$ were added, and the sample was incubated with stirring (for typically ∼2 h) until the 410 nm/280 nm absorption ratio was ∼0.38. The reconstituted protein was then concentrated by ultrafiltration, and the protein concentration was determined by using a Bio-Rad (Hercules, CA) protein assay kit.

Enzyme Inhibition Assays. All assays were performed anaerobically at room temperature according to Altincicek et al.[24] with minor modification. To a pH 8.0 buffer solution containing 50 mM Tris·HCl, 150 mM NaCl, and 5% glycerol, sodium dithionite was added to 0.4 mM, methyl viologen was added to 2 mM, and IspH was added to 72 nM. For enzyme assays, various amounts of HMBPP were added, and the reactions were monitored at 732 nm. The initial velocities were fitted by using the Michaelis−Menten equation with OriginPro 8 (OriginLab Corp., Northampton, MA) software. The activity of reconstituted *A. aeolicus* IspH tested under the conditions described above was 1.2 μmol min^{-1} mg^{-1}, with $K_M = 7\ \mu M$. For inhibition assays, various concentrations of inhibitor were added and incubated for 10 min, prior to addition of 34 μM HMBPP. Initial velocities at different inhibitor concentrations were then plotted as dose−response curves and fitted to the following equation, from which IC_{50} values were determined:

$$y = \frac{1}{1 + (x/IC_{50})^{slope}}$$

where x is the inhibitor concentration and y is the fraction inhibition. K_i values were then deduced from the IC_{50} value by using the Cheng−Prusoff equation:[29]

$$K_i = \frac{IC_{50}}{1 + [S]/K_M}$$

where [S] is the HMBPP concentration and K_M is the Michaelis constant.

EPR Spectroscopy. Samples for EPR spectroscopy were typically 0.3 mM in IspH and were reduced by adding 20 equiv of sodium dithionite followed by incubating for 5 min. Glycerol was added to 42.5% (v/v). EPR samples were frozen in liquid nitrogen after reduction. EPR spectra were collected at X-band using a Varian E-122 spectrometer together with an Air Products (Allentown, PA) helium cryostat. Data acquisition parameters were typically as follow: field center, 3250 G; field sweep, 800 G; modulation, 100 kHz; modulation amplitude, 5 G; time constant, 32 ms; 60 s/scan; 8 s between scans; and temperature, 15 K. EPR spectral simulations were carried out by using the EasySpin program.[30]

Docking Calculations. For docking calculations, the IspH target protein (PDB code 3F7T) was prepared using the protein preparation wizard in Maestro 8.0.[31] Water from the active-site region was removed, as was the diphosphate ligand. The Fe_3S_4 cluster was reconstituted computationally to form the Fe_4S_4 species as described previously,[7] and hydrogen atoms were added to the protein. Hydrogen bonds were optimized to default values, and an energy minimization in MacroModel 9.5[32] was performed only on the protein hydrogens, using default parameters. A receptor grid large enough to encompass all crystallographically observed binding sites was then generated from the prepared target protein. Geometry-optimized ligands were docked using Glide[25] extra-precision (XP) mode, and no other constraints were applied. In some instances, we also used the MMFF94 force field[33] to effect further geometry optimization.

Density Functional Theory Calculations. In order to gain a better understanding of the interaction between the propargyl diphosphate inhibitors and the Fe−S cluster, we used the published

(29) Cheng, Y.; Prusoff, W. H. *Biochem. Pharmacol.* **1973**, *22*, 3099.
(30) Stoll, S.; Schweiger, A. *J. Magn. Reson.* **2006**, *178*, 42.
(31) *Maestro 8.0*; Schrodinger, LLC: New York, 2007.
(32) *MacroModel 9.5*; Schrodinger, LLC: New York, 2007.
(33) Halgren, T. A. *J. Comput. Chem.* **1996**, *17*, 490.

structure of the lowest energy form of allyl alcohol bound to the nitrogenase FeMo cofactor (structure 3 in ref 18), converting Mo → Fe, X → S, and allyl → alkynyl as the initial structure. Geometry optimization was performed by using the pure density functional theory (DFT) method with a BPW91 functional,[34,35] a Wachter's basis (62111111/3311111/3111) for Fe,[36] 6-311G* for all the other heavy atoms, and 6-31G* for the hydrogens, using the Gaussian 09 program.[37] This method is similar to that used in the calculations of the ligand-bound nitrogenase structures[18] and is the same as that we used previously to make accurate predictions of NMR hyperfine shifts and ESR hyperfine couplings, as well as Mössbauer quadrupole splittings and isomer shifts, in various iron-containing proteins and model systems.[38−43]

Synthetic Aspects. General Methods. All reagents used were purchased from Aldrich (Milwaukee, WI). The purities of all compounds investigated were confirmed either via combustion analysis (for solid samples) or by using ^{1}H and ^{31}P NMR spectroscopy at 400 or 500 MHz on Varian (Palo Alto, CA) Unity spectrometers. Cellulose TLC plates were visualized by using iodine or a sulfosalicylic acid−ferric chloride stain.[44] Propargyl methanesulfonate and but-3-ynyl methanesulfonate were synthesized according to a literature method.[45,46] The syntheses and characterization of compounds **18**−**25** have been described previously,[22,47−51] and the samples used here were from the same batches as described.

General Procedure for Preparation of Diphosphates. Diphosphates were prepared using modified literature procedures.[52] Typically, 0.5−1 mmol of halide or mesylate in a minimum amount of CH_3CN (0.4−0.6 mL) was added dropwise to a stirred solution of 2−3 equiv of tris(tetra-*n*-butylammonium) hydrogen diphosphate in CH_3CN (3−6 mL) at 0 °C, and then the reaction mixture was allowed to stir for 2−24 h at room temperature and solvent removed under reduced pressure. The residue was dissolved in cation-exchange buffer (49:1 (v/v) 25 mM NH_4HCO_3/2-propanol) and slowly passed over 60−100 mequiv of Dowex AG50W-X8 (100−200 mesh, ammonium form) cation-exchange resin, pre-equilibrated with two column volumes of the same buffer. The product was eluted with two column volumes of the same buffer, flash frozen, and then lyophilized. The resulting powder was dissolved in 50 mM NH_4HCO_3. 2-Propanol/CH_3CN (1:l (v/v)) was added, and the mixture was vortexed and then centrifuged for 5 min at 2000 rpm. The supernatant was decanted. This procedure was repeated three times, and the supernatants were combined. After removal of the solvent, lyophilization, and then flash chromatography on a cellulose column, a white solid was obtained.

Synthesis of Individual Compounds. Prop-2-ynyl Diphosphate (11). Propargyl methanesulfonate (134 mg, 1 mmol) in CH_3CN (0.5 mL) was added dropwise to a stirred solution of 2.70 g (3.0 mmol) tris(tetra-*n*-butylammonium) hydrogen diphosphate in CH_3CN (4 mL) at −20 °C. The reaction mixture was then slowly warmed to room temperature over 2 h and solvent removed under reduced pressure. Flash chromatography on a cellulose column (4:1:2.4 (v/v/v) 2-propanol/CH_3CN/50 mM NH_4HCO_3) yielded 47 mg (18%) of a white solid: ^{1}H NMR (400 MHz, D_2O) δ 2.68 (s, 1H), 4.38 (d, $J_{H,P}$ = 9.2 Hz, 2H); ^{31}P NMR (162 MHz, D_2O) δ −10.10 (d, J = 20.7 Hz), −7.67 (d, J = 20.7 Hz).

But-3-ynyl Diphosphate (12). But-3-ynyl methanesulfonate (148 mg, 1 mmol) in CH_3CN (0.5 mL) was added dropwise to a stirred solution of 2.70 g (3.0 mmol) of tris(tetra-*n*-butylammonium) hydrogen diphosphate in CH_3CN (4 mL) at 0 °C. The reaction mixture was allowed to warm to room temperature over 24 h and solvent removed under reduced pressure. Flash chromatography on a cellulose column (2:1:1 (v/v/v) 2-propanol/CH_3CN/50 mM NH_4HCO_3) yielded 28 mg (10%) of a white solid: ^{1}H NMR (400 MHz, D_2O) δ 2.16−2.17 (m, 1H), 2.35−2.40 (m, 2H), 3.81−3.84 (m, 2H); ^{31}P NMR (162 MHz, D_2O) δ −9.83 (d, J = 17.0 Hz), −7.82 (d, J = 15.9 Hz).

Pent-4-ynyl Diphosphate (13). Pent-4-ynyl methanesulfonate (162 mg, 1 mmol) was treated with 2.70 g (3 mmol) of tris(tetra-*n*-butylammonium) hydrogen diphosphate in CH_3CN (4 mL). Flash chromatography on a cellulose column (2:1:1 (v/v/v) 2-propanol/CH_3CN/50 mM NH_4HCO_3) yielded 103 mg (35%) of a white solid: ^{1}H NMR (400 MHz, D_2O) δ 1.65−1.70 (m, 2H), 2.13−2.17 (m, 3H), 3.83 (q, J = 6.8 Hz, 2H); ^{31}P NMR (162 MHz, D_2O) δ −9.64 (d, J = 20.9 Hz), −7.76 (d, J = 20.7 Hz).

4-Hydroxybut-2-ynyl Diphosphate (14). 4-Chlorobut-2-yn-1-ol (104 mg, 1 mmol) was treated with 2.70 g (3 mmol) of tris(tetra-*n*-butylammonium) hydrogen diphosphate in CH_3CN (4 mL). Flash chromatography on a cellulose column (2:1:1 (v/v/v) 2-propanol/CH_3CN/50 mM NH_4HCO_3) yielded 71 mg (24%) of a white solid: ^{1}H NMR (400 MHz, D_2O) δ 4.07 (s, 2H), 4.31 (d, $J_{H,P}$ = 6.8 Hz, 2H); ^{31}P NMR (162 MHz, D_2O) δ −10.11 (d, J = 20.8 Hz), −8.85 (d, J = 20.7 Hz).

Cyanomethyl Diphosphate (15). 2-Chloroacetonitrile (76 mg, 1 mmol) was treated with 2.70 g (3 mmol) of tris(tetra-*n*-butylammonium) hydrogen diphosphate in CH_3CN (4 mL). Flash chromatography on a cellulose column (2:1:1 (v/v/v) 2-propanol/CH_3CN/50 mM NH_4HCO_3) yielded 45 mg (17%) of a white solid: ^{1}H NMR (400 MHz, D_2O) δ 4.56 (d, J = 10.4 Hz, 2H); ^{31}P NMR (162 MHz, D_2O) δ −10.25 (d, J = 22.0 Hz), −7.37 (d, J = 20.7 Hz).

2-Cyanoethyl Diphosphate (16). 3-Bromopropanenitrile (134 mg, 1 mmol) was treated with 1.80 g (2 mmol) of tris(tetra-*n*-butylammonium) hydrogen diphosphate in CH_3CN (4 mL). Flash chromatography on a cellulose column (2:1:1 (v/v/v) 2-propanol/CH_3CN/50 mM NH_4HCO_3) yielded 31 mg (11%) of a white solid: ^{1}H NMR (400 MHz, D_2O) δ 2.68 (t, J = 6.4 Hz, 2H), 3.96 (q, J = 6.4 Hz, 2H); ^{31}P NMR (162 MHz, D_2O) δ −10.24 (d, J = 20.7 Hz), −6.21 (d, J = 20.7 Hz).

[[(Prop-2-ynyl)phosphinyl]methyl]phosphonic Acid (17). Propargyl methanesulfonate (134 mg, 1 mmol) was treated with 2.70 g (3 mmol) of tris(tetra-*n*-butylammonium) hydrogen methanediphosphonate in CH_3CN (4 mL). Flash chromatography on a cellulose column (2:1:1 (v/v/v) 2-propanol/CH_3CN/50 mM NH_4HCO_3) yielded 93 mg (35%) of a white solid: ^{1}H NMR (500 MHz, D_2O)

(34) Becke, A. D. *Phys. Rev. A* **1988**, *38*, 3098.
(35) Perdew, J. P.; Burke, K.; Wang, Y. *Phys. Rev. B Condens. Matter* **1996**, *54*, 16533.
(36) Wachters, A. *J. Chem. Phys.* **1970**, *52*, 1033.
(37) Frisch, M.; et al. *Gaussian 09*, Revision A.01; Gaussian, Inc.: Wallingford CT, 2009.
(38) Zhang, Y.; Gossman, W.; Oldfield, E. *J. Am. Chem. Soc.* **2003**, *125*, 16387.
(39) Zhang, Y.; Mao, J.; Godbout, N.; Oldfield, E. *J. Am. Chem. Soc.* **2002**, *124*, 13921.
(40) Zhang, Y.; Mao, J.; Oldfield, E. *J. Am. Chem. Soc.* **2002**, *124*, 7829.
(41) Zhang, Y.; Oldfield, E. *J. Phys. Chem. A* **2003**, *107*, 4147.
(42) Zhang, Y.; Oldfield, E. *J. Phys. Chem. B* **2003**, *107*, 7180.
(43) Zhang, Y.; Oldfield, E. *J. Am. Chem. Soc.* **2004**, *126*, 4470.
(44) Davisson, V. J.; Woodside, A. B.; Poulter, C. D. *Methods Enzymol.* **1985**, *110*, 130.
(45) Jackson, W.; Perlmutter, P.; Smallridge, A. *Aust. J. Chem.* **1988**, *41*, 1201.
(46) Franceschin, M.; Alvino, A.; Casagrande, V.; Mauriello, C.; Pascucci, E.; Savino, M.; Ortaggi, G.; Bianco, A. *Bioorg. Med. Chem.* **2007**, *15*, 1848.
(47) Martin, M. B.; Grimley, J. S.; Lewis, J. C.; Heath, H. T., III; Bailey, B. N.; Kendrick, H.; Yardley, V.; Caldera, A.; Lira, R.; Urbina, J. A.; Moreno, S. N.; Docampo, R.; Croft, S. L.; Oldfield, E. *J. Med. Chem.* **2001**, *44*, 909.
(48) Martin, M. B.; Sanders, J. M.; Kendrick, H.; de Luca-Fradley, K.; Lewis, J. C.; Grimley, J. S.; Van Brussel, E. M.; Olsen, J. R.; Meints, G. A.; Burzynska, A.; Kafarski, P.; Croft, S. L.; Oldfield, E. *J. Med. Chem.* **2002**, *45*, 2904.
(49) Ghosh, S.; Chan, J. M.; Lea, C. R.; Meints, G. A.; Lewis, J. C.; Tovian, Z. S.; Flessner, R. M.; Loftus, T. C.; Bruchhaus, I.; Kendrick, H.; Croft, S. L.; Kemp, R. G.; Kobayashi, S.; Nozaki, T.; Oldfield, E. *J. Med. Chem.* **2004**, *47*, 175.
(50) Sanders, J. M.; Ghosh, S.; Chan, J. M. W.; Meints, G.; Wang, H.; Raker, A. M.; Song, Y. C.; Colantino, A.; Burzynska, A.; Kafarski, P.; Morita, C. T.; Oldfield, E. *J. Med. Chem.* **2004**, *47*, 375.
(51) Szabo, C. M.; Martin, M. B.; Oldfield, E. *J. Med. Chem.* **2002**, *45*, 2894.
(52) Davisson, V. J.; Woodside, A. B.; Neal, T. R.; Stremler, K. E.; Muehlbacher, M.; Poulter, C. D. *J. Org. Chem.* **1986**, *51*, 4768.

δ 2.00 (t, $J_{H,P}$ = 12.0 Hz, 2H), 2.70 (t, J = 2.0 Hz, 1H), 4.37 (dd, $J_{H,P}$ = 9.2 Hz, J = 2.0 Hz, 2H); ^{31}P NMR (202 MHz, D_2O) δ 15.59 (d, J = 9.3 Hz), 20.06 (d, J = 10.7 Hz).

(Pyridin-3-yl)methyl Diphosphate (26). 3-(Bromomethyl)pyridine (86 mg, 0.5 mmol) was treated with 1.35 g (1.5 mmol) of tris(tetra-*n*-butylammonium) hydrogen diphosphate in CH_3CN (3 mL). Flash chromatography on a cellulose column (3:2 (v/v) 2-propanol/50 mM NH_4HCO_3) yielded 73 mg (45%) of a white solid: ^{1}H NMR (400 MHz, D_2O) δ 4.80 (d, $J_{H,P}$ = 7.2 Hz, 2H), 7.31(dd, J = 7.6 Hz, J = 4.8 Hz, 1H), 7.81 (d, J = 7.6 Hz, 1H), 8.30 (d, J = 4.8 Hz, 1H), 8.42 (s, 1H); ^{31}P NMR (162 MHz, D_2O) δ −9.74 (d, J = 22.0 Hz), −5.95 (d, J = 22.0 Hz).

(Pyridin-4-yl)methyl Diphosphate (27). 4-(Bromomethyl)pyridine (86 mg, 0.5 mmol) was treated with 1.35 g (1.5 mmol) of tris(tetra-*n*-butylammonium) hydrogen diphosphate in CH_3CN (3 mL). Flash chromatography on a cellulose column (3:2 (v/v) 2-propanol/50 mM NH_4HCO_3) yielded 65 mg (40%) of a white solid: ^{1}H NMR (400 MHz, D_2O) δ 4.92 (d, $J_{H,P}$ = 8.0 Hz, 2H), 7.41 (d, J = 6.0 Hz, 2H), 8.34 (d, J = 5.6 Hz, 2H); ^{31}P NMR (162 MHz, D_2O) δ −9.66 (d, J = 20.7 Hz), −6.49 (d, J = 20.7 Hz).

(Pyridin-2-yl)methyl Diphosphate (28). 2-(Bromomethyl)pyridine (86 mg, 0.5 mmol) was treated with 1.35 g (1.5 mmol) of tris(tetra-*n*-butylammonium) hydrogen diphosphate in CH_3CN (3 mL). Flash chromatography on a cellulose column (3:2 (v/v) 2-propanol/50 mM NH_4HCO_3) yielded 56 mg (35%) of a white solid: ^{1}H NMR (400 MHz, D_2O) δ 4.91 (d, $J_{H,P}$ = 7.2 Hz, 2H), 7.28 (t, J = 4.8 Hz, 1H), 7.49 (d, J = 8.0 Hz, 1H), 7.80 (t, J = 8.0 Hz, 1H), 8.28 (d, J = 4 Hz, 1H); ^{31}P NMR (162 MHz, D_2O) δ −9.55 (d, J = 22.0 Hz), −6.02 (d, J = 19.4 Hz).

(6-Chloropyridin-3-yl)methyl Diphosphate (29). 5-(Bromomethyl)-2-chloropyridine (103 mg, 0.5 mmol) was treated with 1.35 g (1.5 mmol) of tris(tetra-*n*-butylammonium) hydrogen diphosphate in CH_3CN (3 mL). Flash chromatography on a cellulose column (3:2 (v/v) 2-propanol/50 mM NH_4HCO_3) yielded 70 mg (40%) of a white solid: ^{1}H NMR (400 MHz, D_2O) δ 4.82 (d, $J_{H,P}$ = 7.6 Hz, 2H), 7.29 (d, J = 8.4 Hz, 1H), 7.74 (dd, J = 8.4 Hz, J = 2.4 Hz, 1H), 8.20 (d, J = 2.4 Hz, 1H); ^{31}P NMR (162 MHz, D_2O) δ −9.73 (d, J = 22.0 Hz), −5.81 (d, J = 22.0 Hz).

(Pyridin-3-yl)ethyl Diphosphate (30). 3-(2-Bromoethyl)pyridine (93 mg, 0.5 mmol) was treated with 1.35 g (1.5 mmol) of tris(tetra-*n*-butylammonium) hydrogen diphosphate in CH_3CN (3 mL). Flash chromatography on a cellulose column (2:1:1 (v/v/v) 2-propanol/CH_3CN/50 mM NH_4HCO_3) yielded 42 mg (25%) of a white solid: ^{1}H NMR (400 MHz, D_2O) δ 2.87 (t, J = 6.4 Hz, 2H), 4.00 (q, J = 6.4 Hz, 2H), 7.33 (t, J = 6.4 Hz, 1H), 7.79 (d, J = 8.0 Hz, 1H), 8.24 (s, 1H), 8.36 (s, 1H); ^{31}P NMR (162 MHz, D_2O) δ −9.78 (1 d, J = 20.6 Hz), −7.07 (d, J = 20.6 Hz).

(Pyridin-3-yl)propyl Diphosphate (31). 3-(3-Bromopropyl)pyridine (100 mg, 0.5 mmol) was treated with 1.35 g (1.5 mmol) of tris(tetra-*n*-butylammonium) hydrogen diphosphate in CH_3CN (3 mL). Flash chromatography on a cellulose column (4.5:2.5:3.0 (v/v/v) 2-propanol/CH_3CN/50 mM NH_4HCO_3) yielded 57 mg (33%) of a white solid: ^{1}H NMR (400 MHz, D_2O) δ 1.75−1.89 (m, 2H), 2.65−2.73 (m, 2H), 3.84 (t, J = 6.0 Hz, 2H), 7.34−7.36 (m, 1H), 7.74 (d, J = 8.0 Hz, 1H), 8.26 (s, 1H), 8.35 (s, 1H); ^{31}P NMR (162 MHz, D_2O) δ −9.49 (d, J = 20.7 Hz), −6.87 (d, J = 21.9 Hz).

Acknowledgment. This work was supported by the U.S. Public Health Service (NIH grants AI074233, GM073216, GM65307, and GM085774) and the Mississippi Center for Supercomputing Research. We thank Hassan Jomaa and Jochen Wiesner for providing their *A. aeolicus* IspH plasmid and for initial screening results, Pinghua Liu for the *E. coli* IspH plasmid, and Thomas B. Rauchfuss for helpful discussions.

Supporting Information Available: Complete refs 22 and 37; Table S1, *g*-values reported for Fe_4S_4 proteins and those observed in this study; Figure S1, wide-scan X-band 9 GHz EPR spectra of IspH at 15 K, reduced with $Na_2S_2O_4$. This material is available free of charge via the Internet at http://pubs.acs.org.

JA909664J